Research Square

Preprints are preliminary reports that have not undergone peer review.
They should not be considered conclusive, used to inform clinical practice,
or referenced by the media as validated information.

Therapeutic Potential of Copper-Doped Hydroxyapatite: An Evaluation of Cytotoxicity, Bioactivity, Antimicrobial Efficacy, and Antioxidant Capacity

Hadeel Hasan Khalaf
Mustansiriyah University
Mustafa Shakir Hashim
mustmust@uomustansiriyah.edu.iq

Mustansiriyah University

Research Article

Keywords: Antioxidant, Antimicrobial, anticancer, Hydroxyapatite

Posted Date: November 23rd, 2026

DOI: https://doi.org/10.21203/rs.3.rs-11706443/v1

License: This work is licensed under a Creative Commons Attribution 4.0 International License.
Read Full License

Additional Declarations: No competing interests reported.

Therapeutic Potential of Copper-Doped Hydroxyapatite: An Evaluation of Cytotoxicity, Bioactivity, Antimicrobial Efficacy, and Antioxidant Capacity

Hadeel Hasan Khalaf Mustafa Shakir Hashim*

Physics department, Education College, Mustansiriyah University, Baghdad-Iraq

*Corresponding author email: mustmust@uomustansiriyah.edu.iq

*(ORCID: 0000-0002-0085-6795)

Abstract

This investigation examines the physicochemical, biological, antimicrobial, antioxidant, and selective anticancer attributes of copper-doped hydroxyapatite (Cu-HAp) synthesized using two separate approaches: a wet chemical co-precipitation method (Cu-cHAp) and extraction from natural catfish bones (Cu-bHAp). The effective embedding of Cu^{2+} ions into the apatite matrix was corroborated by structural and chemical characterizations (XRD, EDX, FESEM, and FTIR), which indicated no alteration to its basic crystal structure. Calcination at 600°C induced partial thermal decomposition into tricalcium phosphate (TCP), forming a biphasic composite that was significantly more pronounced in Cu-bHAp due to lattice strain caused by native biogenic co-dopants (Mg^{2+}, Na^{+}, CO_3^{2-}). Biological evaluations demonstrated that Cu-cHAp showed exceptional efficacy in free-radical scavenging through DPPH assays (IC_{50} ranging from 31.5 to 62.5 µg/mL), achieving approximately 95% inhibition at 500 µg/mL and exhibiting extensive antimicrobial activity against Staphylococcus aureus, Staphylococcus epidermidis, Escherichia coli, Klebsiella sp., and Candida albicans, while Cu-bHAp exhibited limited ion release due to matrix encapsulation. In vitro bioactivity assessments in simulated body fluid (SBF) revealed accelerated formation of an apatite layer on Cu-bHAp, attributed to enhanced local release of calcium and phosphate ions from its secondary TCP phase. Furthermore, cytotoxicity testing (MTT assay) showed that Cu-bHAp possesses exceptional biological selectivity, inducing potent, dose-dependent anticancer effects against MCF-7 breast adenocarcinoma cells (~88–90% cytotoxicity at 200 µg/mL, while maintaining high cytocompatibility toward normal human dermal fibroblasts (HDF cytotoxicity <15%). These findings highlight Cu-cHAp as an effective multifunctional antimicrobial/antioxidant coating and Cu-bHAp as a promising bio-resorbable scaffold for targeted bone cancer therapy.

Keywords: Antioxidant, Antimicrobial, anticancer, Hydroxyapatite

Introduction

Because of its strong resemblance to herbal bone in composition and osteoconductive properties, HAp may be a highly promising fabric for long-term usage as a bone implant. Because of its biocompatibility and bioactivity, it is significantly used in many therapeutic packages, such as the healing of injured bones [1].

The significance of ionic substitution in regulating herbal responses is shown by the fact that some super ions promote angiogenesis while others promote osteogenesis. HAp can accept such replacements because of its flexible crystal structure, and several investigations have shown that doping HAp with trace factors significantly enhances its physicochemical properties and natural performance [2].

The resource of the addition/substitution of foreign ions in their form is a method that might drive the development of HAp homes [3]. Additionally, earlier studies have indicated that this may be done by substituting zinc, copper, silver, cerium, and so on. The existing composite materials have advanced residences [4]. For example, modest amounts of copper ions (Cu^{2+}) are very useful for biomedical applications in bone regeneration because they

increase the number of new blood vessels and improve the survival of osteogenic cells in implants, much like antibacterial homes [5]. The law of bone growth and skeleton improvement depends heavily on copper. It eliminates bone free radicals that cause osteoclast activation as a cofactor of antioxidant enzymes [6]. Furthermore, copper instantly prevents osteoclastic bone resorption [7]. All things considered, copper will increase bone electricity and help maintain the highest quality of bone in the country. It has been suggested that copper plays a critical role in the keratinization of hair and fur and collagen stiffening in animals. While copper is essential for bone development and mineralization, it also functions as a cofactor for a number of enzymes, including lysyl oxidase, which is responsible for the go-linking of collagen fibers. A bone weak spot may result from interference with this procedure [8]. The substitution occurring at Ca internet sites or within the interstitial places alongside the hexagonal channel is controlled by the ionic radii of Cu^{+} and Cu^{2+} as well as the doped quantity of Cu [9]. According to some reports, copper is essential for the keratinization of hair and fur and collagen stiffening in animals. Additionally, studies have shown that copper is important for the normalization of calcium (Ca) and phosphorus (P) deposition in bones [10].

For a variety of uses, including fertilization, coloring, bioceramics, and electrocatalysis, copper has been significantly added to apatite-based materials. Copper is widely non-cytotoxic and well-known for its antibacterial and bactericidal properties, which makes it suitable for use in biomedical applications [11]. Several investigations have examined divalent copper's osteoinductive potential, demonstrating its capacity to induce angiogenesis, encourage endothelial mobile proliferation, facilitate collagen and elastin cross-linking in bone tissue, and enhance wound healing [12].

Many attempts have been made over the past few years to obtain potential natural resources for biomaterials. Here, the functioning of HAp derived from animal skeletons has been studied alongside fishes [13]. Natural apatite crystals and traditional synthesized stoichiometric HAp have substantially different residences [14]. The advantage for naturally derived HAp is presence of additional ions such as zinc, magnesium, strontium etc. [15]. A low-cost method of producing HAp from fish bones can likewise get natural HAp consistent with the previous criticisms [16]. Boutinguiza *et al*. verified that HAp obtained from swordfish and tuna bones is not cytotoxic [17].

Besides their regenerating abilities, Cu^{2+} ions have notable antibacterial properties against prevalent pathogens such as Bacillus subtilis, Escherichia coli, and Staphylococcus aureus, through interactions with functional groups in microbial proteins [18]. K.M. Weiss demonstrated that the doped HAp maintained its biocompatibility while exhibiting enhanced antibacterial properties, highlighting the reparative capabilities of ion-substituted apatites [19]. The amalgamation of metals and antibiotics alongside hydroxyapatite can provide synergistic effects, since metal complexes serve as cofactors for antibiotics, occasionally demonstrating superior antibacterial efficacy compared to traditional antimicrobials [20]. Copper ions' ability to produce reactive oxygen species (ROS) that harm microorganisms has been linked to their antibacterial properties [21]. Additionally, copper ions can interact with DNA by disrupting metabolic processes and interfering with nucleic acid strands [22]. Additionally, intracellular hydroxyl radicals produced by copper ions can harm vital proteins [23]. Although the exact processes underlying the antibacterial activity of copper ions are still being studied, there is enough evidence to support the idea that ion launch, reactive oxygen species, and direct contact killing are the causes [24].

Oxidative stress has emerged as a fundamental factor in human health, resulting from the excessive generation of reactive oxygen species (ROS) relative to the capacity of the body's antioxidant defenses. Comprehending the interaction of ROS with freshly integrated bone is essential for enhancing the ultimate outcomes of implants and recovery methods following surgeries involving implants. Copper ions has the capability to protect cells from oxidative stress, assist in adenosine triphosphate (ATP) production via the mitochondrial electron transport chain, and promote the cross-linking of collagen and elastin, which is crucial for tissue integrity. The use of copper as a doping agent is an intriguing prospect because of the redox properties that might enhance the antioxidant characteristics of HAp [27].

The bioactivity of HAp facilitates the generation of new bone by biochemical adhesion at the interface of the bone implant. Copper ions have been indicated to enhance angiogenesis and promote endothelial cell proliferation both in vitro and in vivo [28]. It was reported that bioactivity assessments demonstrated that fish-derived hydroxyapatite produces more new apatite than synthetic hydroxyapatite following a 7-day incubation in SBF [29].

This study aims to 1) Synthesize Cu-cHAp and Cu-bHAp to investigate how origin impacts material properties, 2) Evaluate the bioactivities of both samples by testing apatite layer deposition in SBF, 3) Screen DPPH free-radical scavenging capacity to test the material's ability to mitigate oxidative stress, 4) Determine screen inhibition zones against Gram-positive, Gram-negative, and fungal pathogens, and 5) Test cytocompatibility on normal human dermal fibroblasts (HDF) alongside selective anti-cancer activity against MCF-7 breast adenocarcinoma cells.

Experimental part

1- Preparation of materials and characterization

Copper doped HAp nanoparticles were made via co-precipitation method with slight modifications [30]. At the outset, 0.1 mol of calcium nitrate tetrahydrate (HIMEDIA, INDIA) and 0.06 mol of diammonium hydrogen phosphate (HIMEDIA, INDIA) were dissolved in deionized water, and the pH of each solution was modified to 10 using ammonia. Following one hour of stirring, the phosphate solution was introduced to the calcium nitrate solution dropwise, while maintaining the pH within the range of 10. The milky solution was agitated on a stirrer for 24 hours and subsequently aged for 48 hours at ambient temperature to get particles with a consistent shape. The solution was subsequently centrifuged to separate the supernatant water from the apatite gel, and the gel was then washed three times with distilled water to remove any residual ammonia and nitrate. The obtained gel was subjected to drying in a vacuum oven at 70 °C for about 72-96 hours until fully dehydrated before being ground in a mortar. The fabrication of copper doped HAp was executed as previously described, except that copper nitrate hexahydrate (HIMEDIA, INDIA) was dissolved in 20 ml of deionized water at specified concentrations and subsequently added to the calcium nitrate solution after adjusting the pH to 10. To examine the impact of heating on the morphology and crystalline structure of HAp, the dehydrated HAp powders were then subjected to calcination at 600 °C for 2 hours.

The natural raw material used as a source of hydroxyapatite was obtained from catfish bone according to the following procedure. The fish bones were boiled in water for 1 h and washed using a strong water jet to eliminate the fish meat, boiling and washing processes were repeated several times to obtain pure bones. The milling process was done by using milling machine (Retczh PM40 Germany) to obtain fine fishbone. The milling duration by this machine was eight hours, the number of milling container rotation was 200 cycle/minute. Calcination of fishbone particles were carried out after milling process by using furnace [Hermann- Moritz, Italy]. Heat treatment was done under inert gas (argon) during two hours at 600 C. Copper doped bone derived hydroxyapatite (Cu-bHAp) was prepared using a wet chemical treatment approach, in which copper nitrate was introduced into the previously extracted bone derived hydroxyapatite powder. Initially, 5 g of the previously prepared bHAp powder was used as the starting material. The copper precursor was copper nitrate, which served as a soluble source of Cu^{2+} ions. Copper nitrate was selected because of its solubility in aqueous media and its suitability as a precursor in the preparation of copper containing hydroxyapatite materials. The required amount of copper nitrate corresponding to the intended nominal copper concentration of 5% was prepared separately by dissolving the salt in the appropriate solvent. Meanwhile, the bHAp powder was dispersed in a separate portion of the preparation medium under continuous magnetic stirring to obtain a homogeneous suspension. The copper nitrate solution was then gradually introduced into the bHAp suspension under continuous stirring.

After completing the addition, the resulting mixture was maintained under continuous stirring to promote interaction between the copper ions and the calcium phosphate-based particles. Following the treatment, the resulting solid material was separated from the liquid phase and subjected to washing with distilled water to remove residual soluble salts, unreacted copper nitrate, and other impurities.

All specimens were analyzed utilizing the segment assessment instrument (XRD-Shimadzu 6000 X-ray diffractometer). The utilized SEM apparatus is the FESEM MIRA3 TESCAN, originating from France. FTIR analyzes have been conducted with the Spectrum N equipment from PerkinElmer Inc.

2- **Biological tests**

2-1 Bioactivity test

In vitro bioactivity test become performed with the aid of the use of simulated frame fluid (SBF; pH = 7.4), prepared by means of the changed Kokubo and Takadama approach [31].

2-2 Microbial test

The methodology for evaluating the antibacterial properties of the samples against harmful microorganisms was reported by [32]. Inhibition zones were measured in millimeters.

The specimens were evaluated for their antibacterial effects against pathogenic bacteria (Staphylococcus aureus, Staphylococcus epidermidis, Escherichia coli, Klebsiella sp., and Candida albicans). These isolates have been collected from the Department of Biology, College of Science, Mustansiriyah University. The plates were arranged by dispersing about 10^5 CFU/mL of the culture broth of each indicator bacterial isolate onto the nutrient agar surface. The agar plates have been left for about 15 minute in advance before aseptically distributing the 50µL of the tested samples into the agar wells already drilled in the agar plates. The plates were subsequently incubated at 37 °C for a duration of 18 to 24 hours.

2-3 Antioxidant test

The antioxidant capacity of the samples was measured using the free DPPH radical suppression method, according to a modified standard protocol. This method relies on the samples' ability to neutralize free DPPH radicals, an effect measured by the decrease in absorbance at 517 nm. Spectral readings were performed using (Beckman Coulter, Inc.,USA), ensuring the instrument was calibrated before measurements began. A working solution of DPPH was prepared at a concentration of (2.366 mg dissolved in 100 ml of absolute methanol). The samples under test were then diluted at seven sequential concentration levels (500, 250, 125, 62.5, 31.25, 15.6 µg/ml) to ensure an accurate and comprehensive measurement range for assessing antioxidant activity.

The examination was conducted utilizing two primary groups: a sample group and a negative control group. Sample group: Equal quantities of the operational DPPH solution were combined with the sample solution at each designated concentration. The operational DPPH solution was combined with an equivalent amount of pure methanol (without the sample) to illustrate the peak free radical absorption devoid of any inhibitory influence. All combinations were allowed to incubate in the absence of light at ambient temperature for 30 minutes (or the duration indicated in the procedure).

2-4 Anticancer test

The information from this verification is cited using the valuable source of [33]. The cytotoxic effects of several chemicals isolated from L. Camara crude extracts were assessed using a ready-to-use MTT kit (Intron Biotech). The kit comprises: MTT solution in ten 1 ml vials and solubilization solution in two 50 ml bottles. Tumor cells (1×10^4 to 1×10^6 cells/ml) were cultivated on ninety-six well flat-bottom microtiter plates, with a final volume of 200 µl of complete culture media per well. The microplate was covered with sterile parafilm and gently shaken. The plates were incubated at 37°C with 5% CO_2 for 24 hours. Subsequent to incubation, the medium was discarded, and fold serial dilutions of the well-known chemical (12.5, 25, 50, 100, 200, and 400 µg/ml) were added to the wells. Triplicates were employed for each recognition alongside the controls (cells treated with serum-free media). Plates were maintained at 37°C with 5% CO_2 for the designated exposure duration of 24 hours. Subsequent to the

publicity, 10 µl of the MTT solution is administered to each appropriately. Plates were likewise incubated at 37°C with 5% CO_2 for a duration of four hours. The media were carefully extracted, and 10µl of solubilization solution was introduced, ensuring uniformity for 5 minutes. The Michigan Cancer Foundation-7 (MCF-7) cell line was established from the pleural effusion of a 96-year-old female with breast cancer (Soule, 1973). This mobile line was transformed into one obtained from the Center of Biotechnological Research. Number of passages: 15.

A one-way analysis of variance (ANOVA) using Duncan's method was conducted to determine the significance of group variance, with statistical significance defined as ($p \pm 0.05$). Data were presented as mean ± standard deviation, and statistical analyzes were conducted using Graph Pad Prism version 6 (Graph Pad Software Inc., La Jolla, CA).

We will refer to the prepared samples with the following symbols:

Sample Description	Symbol
Chemically prepared pure HAp	cHAp
Chemically prepared Cu-doped HAp	Cu-cHAp
pure HAp (catfish)	bHAp
Cu-doped (Catfish bone)	Cu-bHAp

Results and discussions

Structural properties

Figure 1 illustrates XRD patterns of cHAp, Cu-cHAp and Cu-bHAp samples. The major diffraction peaks of the synthesized samples were found to coincide with the characteristic reflections of HAp, confirming the preservation of the apatite crystal structure after copper incorporation. The most intense reflections observed in the region of $2\theta \approx 31–33°$ correspond to the typical HAp phase and indicate successful phase formation. Slight variations in peak intensity and broadening were observed compared with the standard pattern. These changes may be attributed to lattice distortion caused by the substitution or incorporation of Cu ions within the HAp crystal lattice. The broad diffraction peaks further suggest the nanocrystalline nature of the synthesized material. The obtained results demonstrate that copper incorporation did not significantly alter the fundamental apatite framework, while inducing minor structural modifications that may influence the physicochemical and biological properties of the material. The XRD results suggest successful copper incorporation; however, elemental analysis and spectroscopic characterization were used to further confirm the presence of Cu ions.

Inside XRD patterns of Cu-cHAp and Cu-bHAp samples, Tricalcium Phosphate (TCP) phase is coexistence with apatite phase. The presence of this phase indicates to the decomposition of HAp when the samples calcified at 600^0C. Probable reaction to produce TCP is as following [34]:

$$Ca(OH)_2 + 2CaHPO_4 \rightarrow Ca_3(PO_4)_2 + 2H_2O$$

Reflections associated with TCP are visibly more pronounced in the Cu-bHAp profile than in Cu-cHAp, indicating increased phase transformation or non-stoichiometry in the bone-derived sample.

Gopi *et al.* state that, to enhance the biomaterial properties, they may be combined with different substances, like TCP [35]. TCP is a biocompatible material that promotes new bone development by releasing calcium and phosphate ions; it also rapidly disintegrates when exposed to bodily fluids [36].

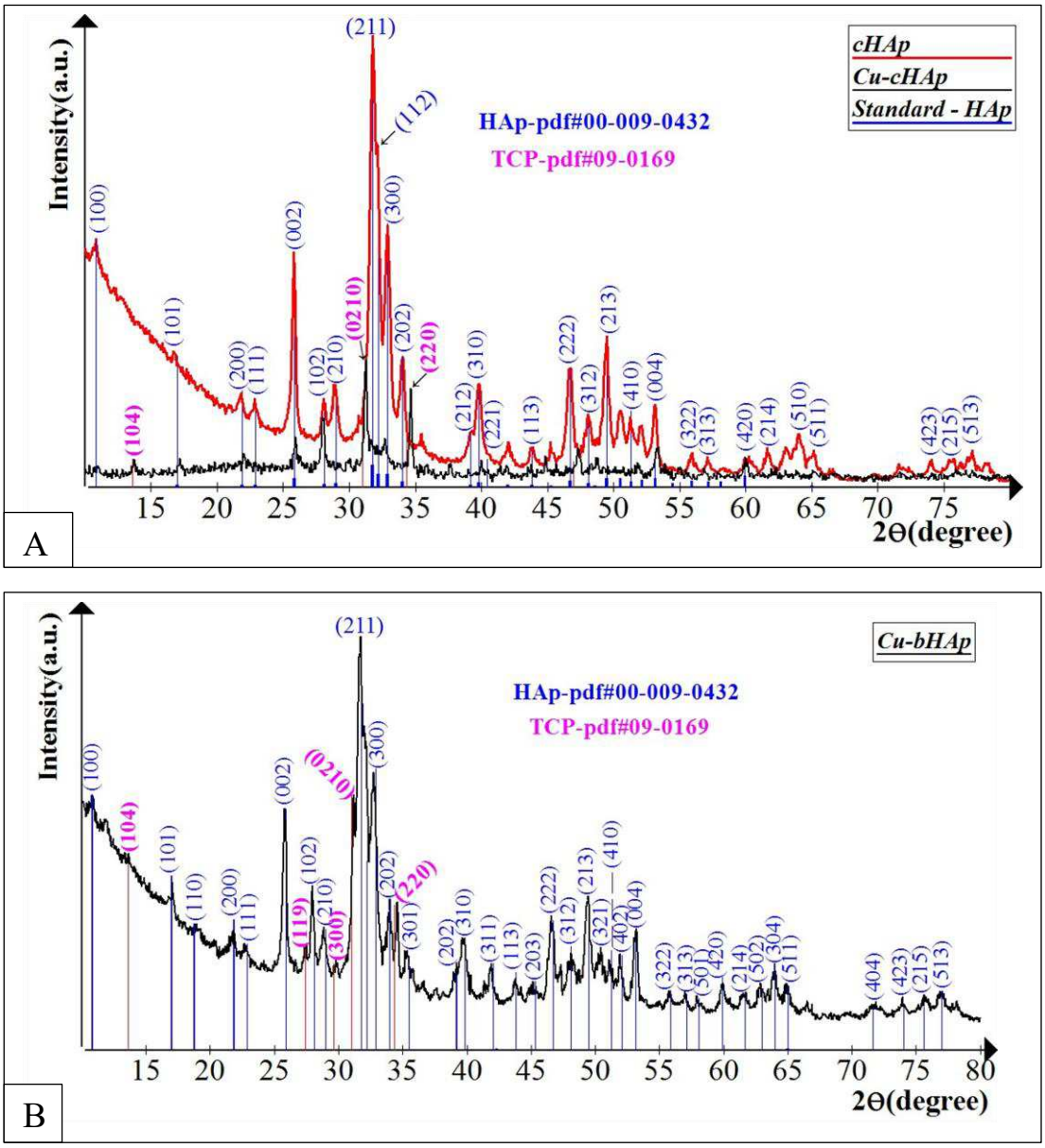
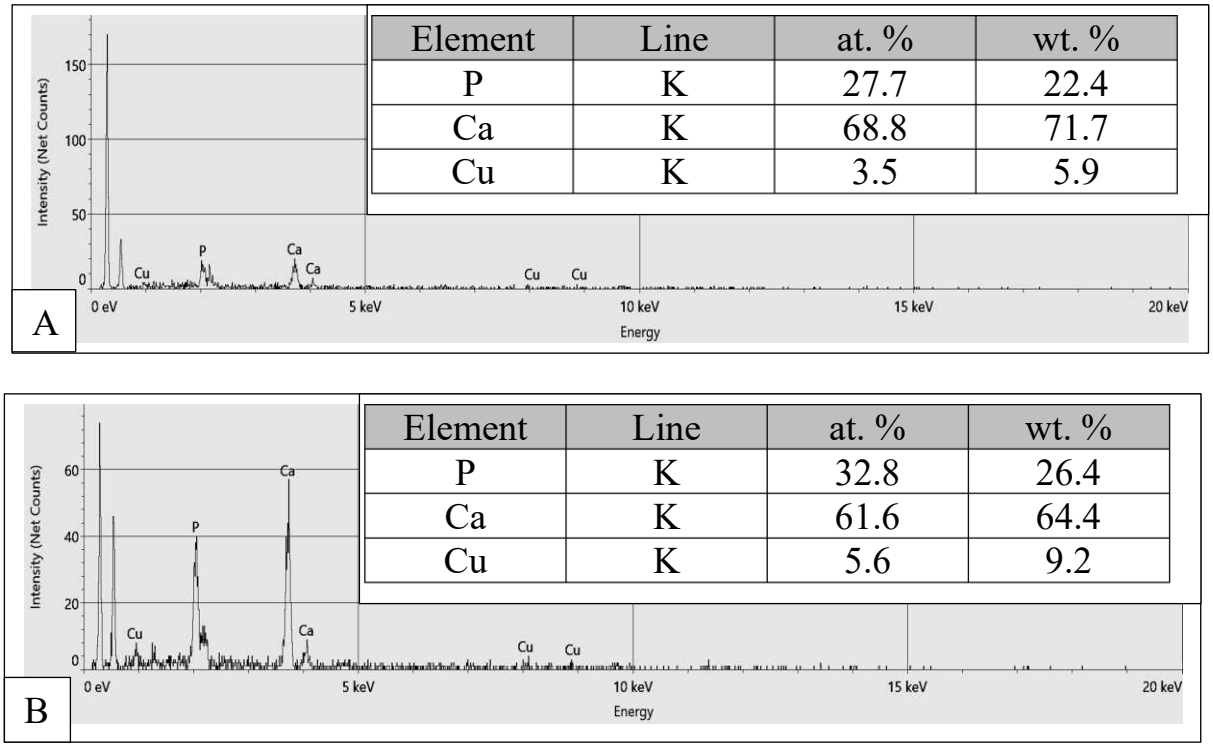


Fig1. XRD patterns of: A) Cu-cHAp and B) Cu-bHAp.

Catfish bones naturally contain trace ions (like Mg^{2+} and Na^{+}) and organic components. During the high temperature calcination process used to extract HAp from natural bone, these ions destabilize the HAp lattice, promoting partial thermal decomposition of HAp into TCP. Synthetic chemical preparation (Cu-cHAp), by contrast, allows for tighter stoichiometric control (Ca/P≈ 1.67), keeping the phase highly pure with minimal TCP transformation.

Figure 2 shows EDX spectra for Cu-cHAp and Cu-bHAp samples with inset tables contain at% and wt% .



Element	Line	at. %	wt. %
P	K	27.7	22.4
Ca	K	68.8	71.7
Cu	K	3.5	5.9

Element	Line	at. %	wt. %
P	K	32.8	26.4
Ca	K	61.6	64.4
Cu	K	5.6	9.2

Fig2. EDX spectrum for A: Cu-cHAp and B: Cu-bHAp.

According to the inset table (Figure 2.A), Cu-cHAp has a much higher cation to phosphorus ratio (~2.61), placing it far above the 1.5 required TCP formation. This confirms high chemical stability and supports the XRD finding. On the other hand**,** Cu-bHAp contains significantly lower ratio (~2.05) with a higher phosphorus proportion (32.8 at.%) . A phosphorus rich shift brings the composition closer to calcium deficient TCP favoring stoichiometry (1.5), consistent with the secondary TCP phase seen in XRD.

Cu-bHAp displays a heavily calcium rich non stoichiometric surface. This lattice distortion forces copper ions to reside primarily on accessible surface coordination sites rather than deep inside the crystal matrix. For Cu-bHAp , closer to the ideal stoichiometry, copper is tightly bound or substituted deep inside the calcium deficiency/lattice matrix, rendering it sterically hidden or inactive.

Maps A, B, C (Cu-cHAp) and D, E, F (Cu-bHAp) in figure 3 show a highly uniform, dispersed distribution of calcium, phosphorus, and copper without micro-segregation. The lack of localized "clusters" or localized bright spots indicates that copper ions are evenly integrated throughout the HAp matrix rather than forming separate phase precipitates such as isolated $Cu(OH)_2$ nanoparticles.

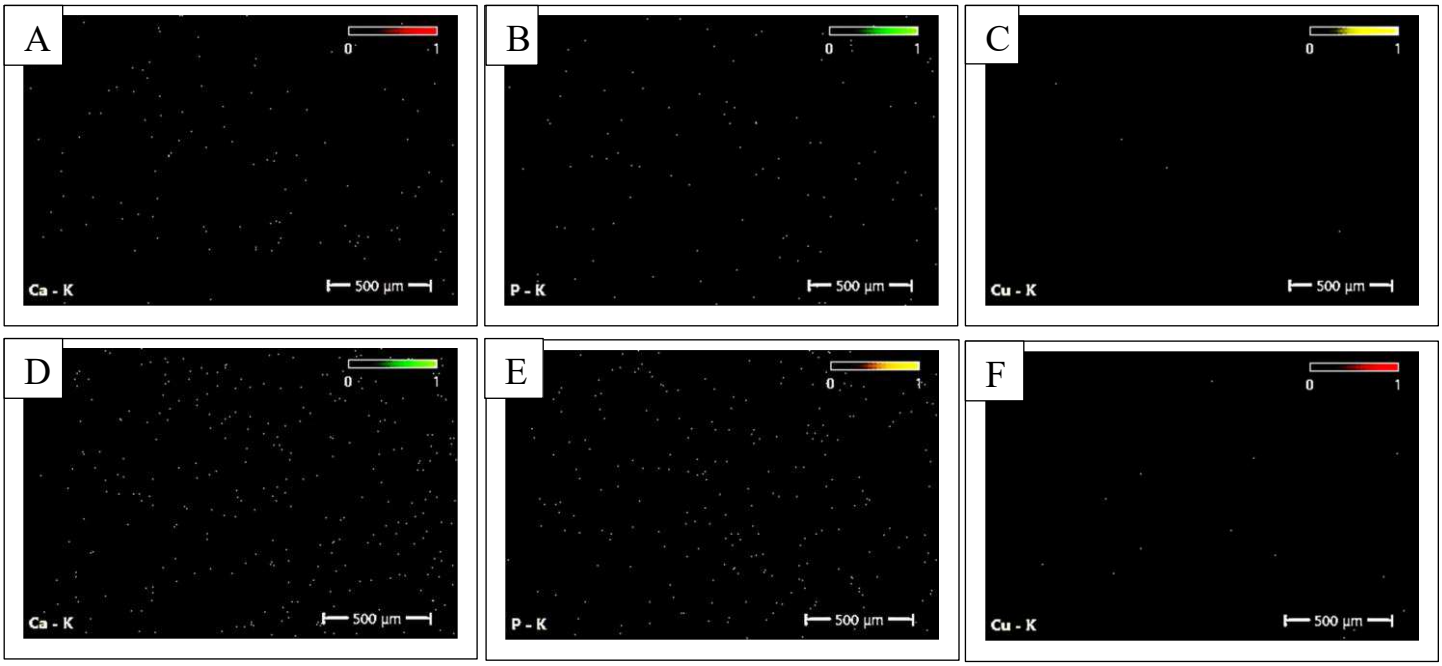


Fig 3. **Maps for elements distribution :A,B, and C for Cu-cHAp. D, E, and F for Cu-bHAp**

Biological HAp naturally contains structural carbonate ions (CO^{2-}_3), as confirmed in FTIR spectrum (Figure 4). Carbonate substituting for phosphate (PO^{3-}_4) or hydroxyl (OH^-) groups creates charge imbalances and lattice strain. These lattice defects create additional vacancy sites and lower the thermodynamic energy barrier for metal cation exchange, allowing significantly more Cu^{2+} ions to substitute into the structure during synthesis [34]. The abundance of pre-existing calcium vacancies (Ca^{2+} vacancies) provides readily available sites into which incoming Cu^{2+} ions can easily bind. On the other hand, chemically synthesized HAp forms a stoichiometric or calcium-rich crystal lattice. Without preexisting structural vacancies, the lattice resists ion substitution, capping the maximum uptake of copper.

The FTIR spectra of both samples, as seen in figure 4, validate the establishment of the HAp structure and the effective integration of copper species. The pronounced absorption band seen in the range of 1000–1100 cm^{-1} is ascribed to the asymmetric stretching vibration (v^3) of the phosphate group (PO_4^{3-}), a distinctive characteristic of HAp [37]. Another phosphate related absorption band seen in the 500–600 cm^{-1} range relates to the bending vibration (v^4) of PO_4^{3-} ions.

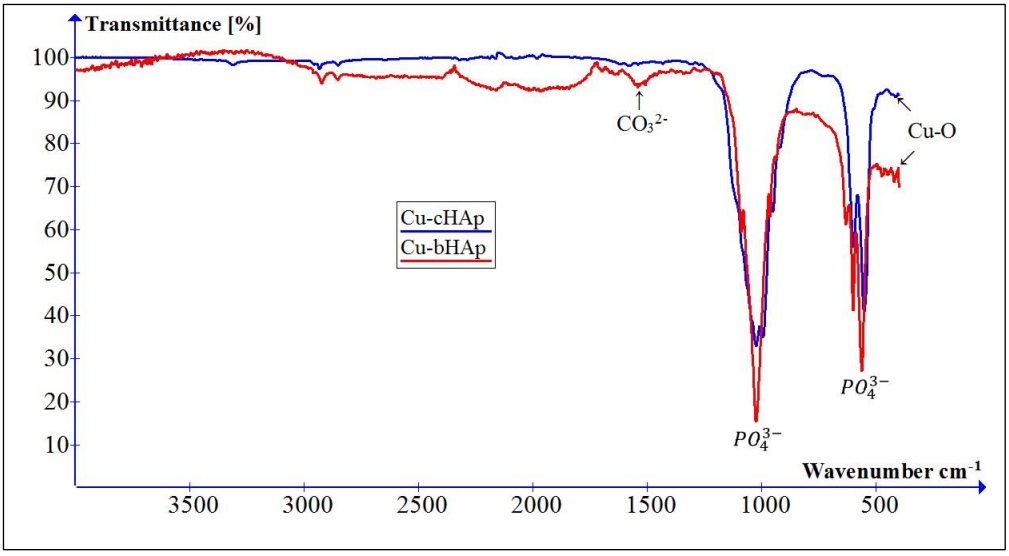


Fig 4. FTIR spectrum of Cu-cHAp and Cu-bHAp samples.

A weak absorption band located within the lower wavenumber location around 500–600 cm^{-1} may be assigned to the Cu–O bond vibration, indicating the presence of copper-containing species inside or on the HAp matrix. The protection of the phosphate bands together with the arrival of the Cu–O vibration suggests that copper incorporation did not break the apatite crystal framework.

Furthermore, the peaks at 1028 and 1093 cm^{-1} correspond to the v_3 asymmetric stretching modes of phosphate structures, which are particularly sensitive to lattice distortion, crystallinity, and ionic substitution. The extraordinarily sharp nature of those bands shows an immoderate degree of structural order, whilst the minor band broadening and subtle height shifts advocate the presence of localized lattice distortions triggered with the aid of Cu incorporation, without disrupting the long-range apatite form [38]. Cu-bHAp displays minor broad absorption dips and small peaks in the 2000–3000 cm^{-1} (organic/hydrocarbon region), whereas Cu-cHAp remains flat near 100% transmittance across this region.

The SEM images in Figure 5 reveal that the Cu-cHAp hydroxyapatite particles exhibit a predominantly irregular morphology, with some particles appearing polyhedral in shape. However, the particles are generally neither spherical nor needle-like. The measured particle size ranges from approximately 60 to 150 nm, confirming the nanoscale nature of the synthesized material. The particles are not well separated and show noticeable agglomeration throughout the images. This level of cluster is very public for HAp synthesized via wet chemical methods, where high surface energy drives nanoparticles to cluster together. Furthermore, the particle surfaces appear rough rather than smooth.

Both samples form a highly disordered, random, and interconnected network of large spaces and channels. In biomaterials, macro porosity and interconnected voids are highly desirable. If this material is utilized for coatings or bone scaffolds, these larger spaces allow for protein adsorption, body fluid movement, and cell migration and blood vessel growth. The total specific surface area of the powder is increased by the fine nano porosity.

Based on the visible features in figure 5, both samples appear as hierarchical, highly porous, granular aggregates with a high surface area. The fundamental building blocks for both are irregular nanoparticles fused together, giving the larger clusters a coral or cauliflower-like appearance.

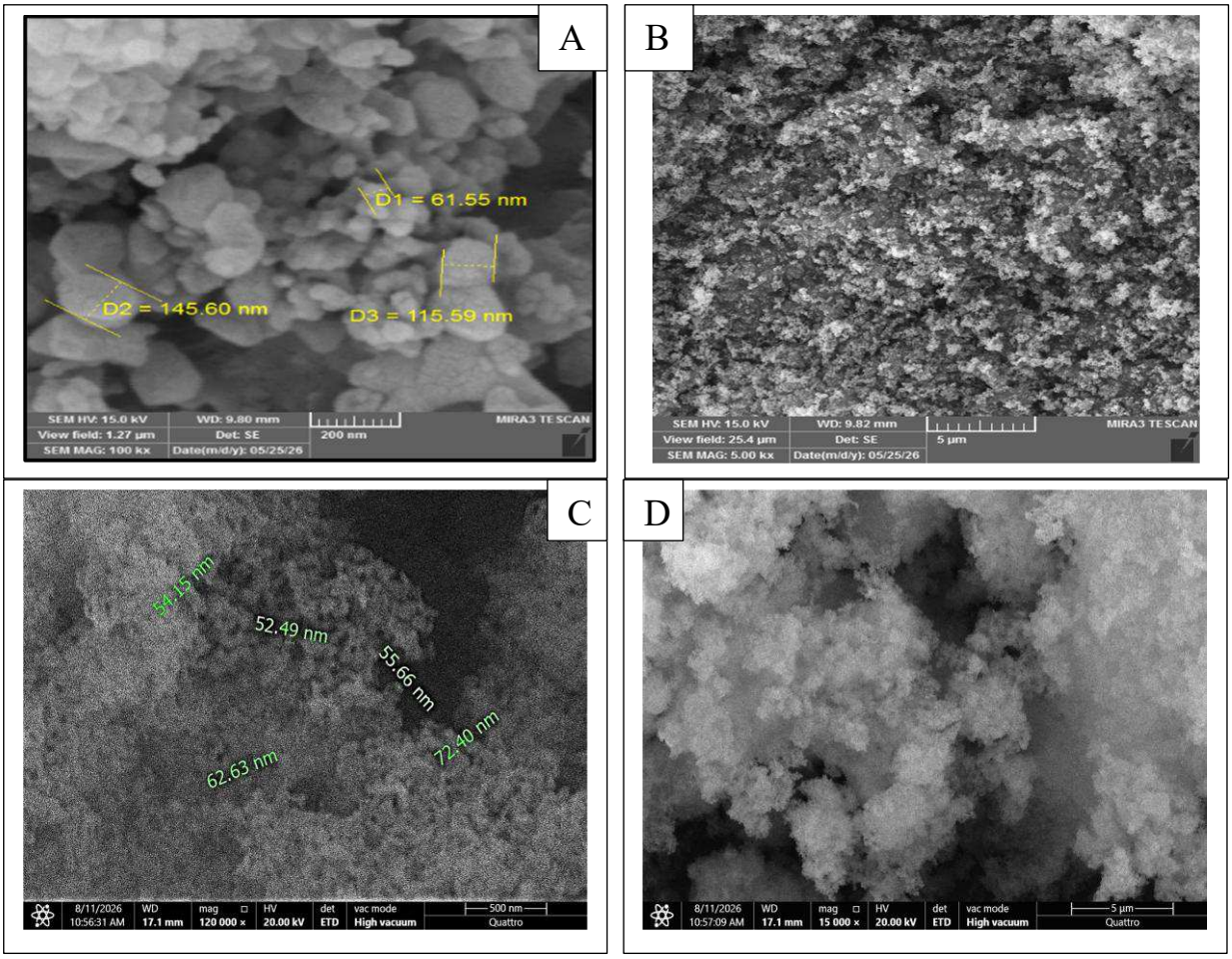


Fig 5. SEM images for :A and B for Cu-cHAp. C and D, for Cu-bHAp.

The results of Antioxidant Test

The diagram in Figure 6 demonstrates a significant, dose-dependent rise in free radical scavenging activity for Cu-cHAp. As the quantity of this substance increases from 15.625 µg/mL to 500 µg/ml, the scavenging activity progressively increases. Cu-cHAp has a very high baseline scavenging activity of about 48% even at the lowest concentration of 15.625 µg/ml. The IC_{50} value (the dose needed to scavenge 50% of the free radicals) is very encouraging. The scavenging activity approaches saturation at around 95% at the highest dose of 500 µg/ml, indicating almost total suppression of the target radicals. This outcome is consistent with [27]. Copper ions (Cu^{2+}/Cu^{+}) function as redox active centers, through a surface-mediated redox cycle, these ions may readily give or take electrons to neutralize free radicals (such reactive oxygen species or DPPH), transforming unstable radicals into stable molecules.

Fabrication of Cu-cHAp powder in the nanometer scale, see figure 5, exponentially increases its specific surface area. This high surface area to volume ratio results in a much denser population of active copper locations, and surface OH groups are exposed on the exterior, allowing for quick, highly effective reaction and contact with the radical species in solution. This makes this material a highly hopeful applicant for biomedical requests where mitigating oxidative stress is crucial (e.g., wound healing coatings or bone tissue engineering).

On the other hand, there is relatively a low scavenging activity for the Cu-bHAp sample at different concentrations. The lower antioxidant activity of Cu-bHAp (~38%) relative to Cu-cHAp (~95%) is attributed to intrinsic lattice phenomena rather than poor dispersion. The presence of biogenic trace ions and the secondary TCP

phase in catfish-bone HAp may tightly bind the dispersed copper ions within the crystal framework, raising the activation energy for electron transfer and restricting DPPH radical interaction [39]. Bone-derived HAp intrinsically contains biological co-dopants (such as Na^{+} , Mg^{2+}, and CO^{2-}_{3} carbonate substitutions). The presence of these native trace ions alters the surface charge density and creates local electrostatic barriers that sterically or electrostatically inhibit large, bulky organic radicals (like DPPH) from approaching the active copper redox sites on the surface.

It may suggest that higher ionic/covalent coordination occurs inside the lattice for the copper ions integrated into the TCP phase matrix. The activation energy needed for redox cycling ($Cu^{2+} \leftrightarrow Cu^{+}$) is increased because these copper species are confined in a tighter crystal field while being evenly distributed. The rate of calcium phosphate dissolution and the amount of substituted ions may be used to calculate the release rate of copper ions doped-HAp [40]. Therefore, it can be said that the Cu-bHAp sample has limitations on the release of copper ions and subsequent enhancement of antioxidant qualities.

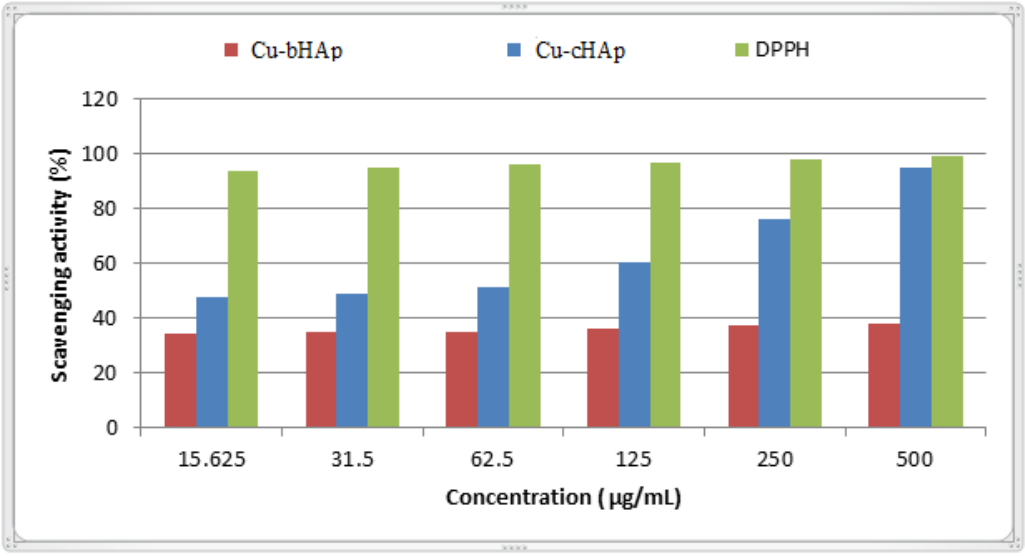


Fig 6. Scavenging activity (%) for both samples.

The result of Antibacterial activity test

The antibacterial activity of Cu-cHAp was assessed against Gram-positive bacteria, Gram-negative bacteria, and the fungal strain Candida albicans using the agar well diffusion technique. In Table 1, the results confirmed that Cu-cHAp shows inhibitory activity against all tested microorganisms. The maximum zone of inhibition was detected against Staphylococcus aureus, with a diameter of 25 mm, indicating that this strain was the most susceptible to the manufactured material. These results confirm that Cu-cHAp has wide spectrum antimicrobial activity against all tested microorganisms.

Across all verified microorganisms, there is a strong concentration dependent tendency. As the concentration of the Cu-cHAp increases from 125 to 500 µg/ml, the inhibition zone expands steadily. The material displays varying levels of effectiveness depending on the species, with a remarkable tendency toward Gram-positive bacteria.

Among the bacteria, E. coli had the smallest zones of inhibition, measuring between 11 and 14 mm. This reduced susceptibility is common for Gram-negative bacteria, such as E. coli. Compared to the porous peptidoglycan cell wall of Gram-positive bacteria like S. aureus, the outer lipid membrane of E. coli frequently functions as a more efficient barrier against metal ions.

The copper's antibacterial properties are a result of several mechanisms, including the disruption of bacterial membrane integrity, the generation of free radicals, and the change of enzyme structure and bacterial protein [41]. S. Aureus bacteria are more resistant to Cu-containing HAp nanoparticles, as demonstrated by Noori et al. According to this study, the growth of S. Aureus bacteria was not entirely stopped by HAp-Cu 2%. It definitely stopped E. Coli growth at a 200 mg/ml dosage. Additionally, HAp-Cu 5% at a dosage of 100 mg/ml entirely prevented the growth of E. Coli, although a greater concentration of 200 mg/ml of the aforementioned powder was needed to suppress the growth of S. Aureus [42].

Table1. Inhibition zones of Cu-cHAp

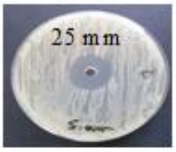
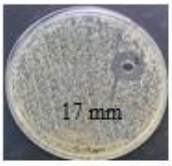
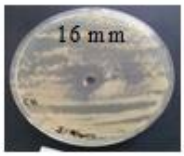
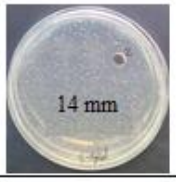
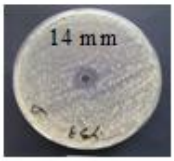
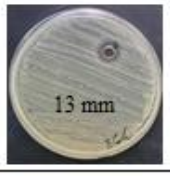
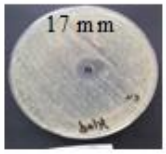
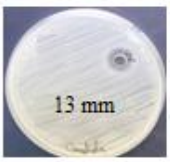
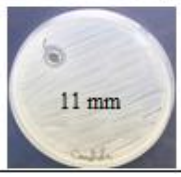
Microorganism	500 µm/ml	250 µm/ml	125 µm/ml
Staphylococcus aureus			
Staphylococcus epidermidis			
Escherichia coli			
Klebsiella sp.			
Candida albicans			

Table 2 illustrates the inhibition zone for all samples (the images are not shown). Unlike the chemical variant where copper incorporation significantly enhances antibacterial performance, Cu-bHAp shows virtually no improvement upon copper addition. Again, this suggests that copper incorporation into catfish bone-derived HAp may be limited, or that the bio-matrix structurally encapsulates the copper ions, preventing active ion release into the agar.

bHAp displays slightly elevated baseline activity compared to cHAp, likely due to natural trace elements present in fish bone ash (such as Mg, Na, or carbonate ions). All samples demonstrate a consistent concentration-dependent decrease in inhibition zone size moving from column 1 (highest concentration) to column 3 (lowest concentration).

Table 2 inhibition zone for all samples

Microorganism		500 µg/ml	250 µg/ml	125 µg/ml
Staphylococcus aureus	cHAP	10	10	10
	Cu-cHAp	25	17	14
	bHAP	17	11	10
	Cu-bHAp	12	11	10
Staphylococcus epidermidis	cHAP	10	11	11
	Cu-cHAp	16	14	12
	bHAP	16	10	11
	Cu-bHAp	12	11	10
Escherichia coli	cHAP	11	11	10
	Cu-cHAp	14	13	11
	bHAP	14	10	11
	Cu-bHAp	14	10	10
Klebsiella sp.	cHAP	10	11	9
	Cu-cHAp	17	15	12
	bHAP	13	10	9
	Cu-bHAp	14	11	9
Candida albicans	cHAP	11	10	11
	Cu-cHAp	18	13	11
	bHAP	15	11	10
	Cu-bHAp	13	10	9

The result of Bioactivity test

The XRD spectrum of Cu-cHAp sample (Figure 7 (A)) is heavily dominated by strong, sharp substrate reflection peaks belonging to metallic titanium, such as (100), (101), and (201). The characteristic hydroxyapatite triplet (211), (112) , (300) around $2\Theta \approx 31^0$–33^0 is extremely weak and barely visible as minor, low-intensity dips/peaks. This indicates that the newly deposited apatite layer on Cu-cHAp is relatively thin, allowing the underlying titanium substrate to dominate the diffraction signal.

XRD pattern of Cu-bHAp **(**Figure 7(B)**)** shows significantly stronger, distinct diffraction peaks that are indicative of the HAp phase. There are noticeable prominent HAp peaks throughout the spectrum, including (002) at $2\Theta \approx 26^0$, a broad primary cluster for (211), (112), and (300) around 31^0-33^0, as well as higher-angle reflections such as (113), (222), and (213). The presence of multiple, distinct HAp crystal plane reflections indicates the formation of a thicker, more crystalline, and structurally mature apatite layer covering the substrate. The biological origin of Cu-bHAp (catfish bone) naturally contains trace co-dopants (such as Mg^{2+}, Na^{+}, and carbonate groups CO^{2-}_{3}) and a higher proportion of secondary tricalcium phosphate (TCP) [1]. The presence of TCP increases local calcium and

phosphate ion release into the SBF solution, thereby accelerating nucleated growth of new biomimetic apatite crystals compared to the synthetic Cu-cHAp sample. This result is in agreement with [43].

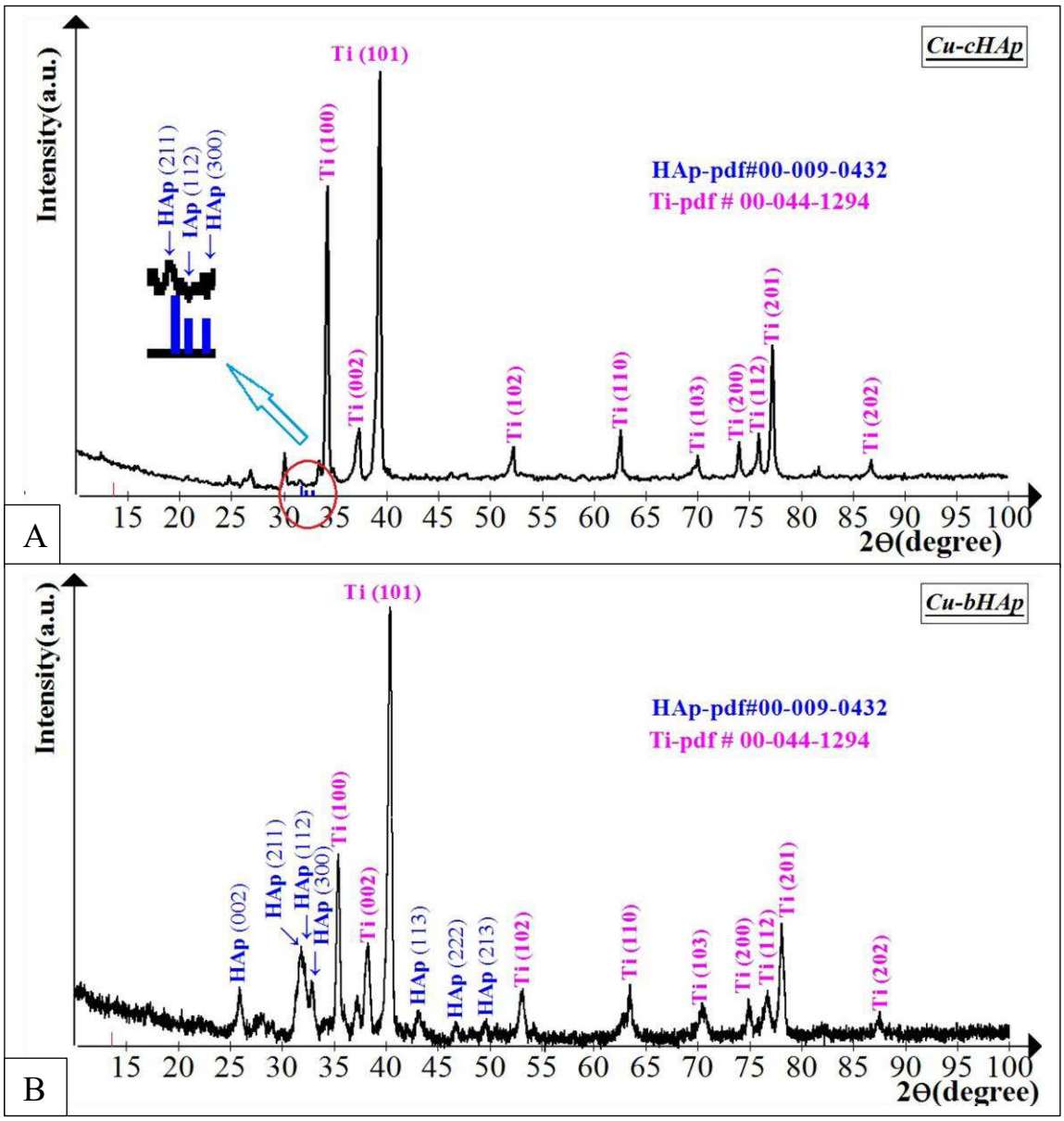


Fig 7. XRD patterns of A: Cu-cHAp and B:Cu-bHAp after immersing inside SBF

The structural and morphological evaluation of both Cu-cHAp and Cu-bHAp following immersion in SBF reveals a clear complementarity between SEM and XRD analyses. SEM images of both samples (Figure 8) clearly confirm the successful nucleation and growth of a fine, interconnected apatite layer composed of uniform spherical to oval nanoparticles. EDX test , see Figure (9A), further verifies the biomimetic composition of this layer through key constituent peaks (Ca ,P, O and Cu), yielding a calcium-deficient Ca/P ratio of 1.53 indicative of successful Cu^{2+} lattice incorporation. Cu-bHAp displays significantly higher Ca and P concentrations compared to Cu-cHAp sample, see (Figure (9B)). This shows that Cu-bHAp induces considerably greater biomimetic HAp precipitation on its surface, indicating superior in vitro bioactivity. Ca/P molar ratios are 1.53 and 1.62 for Cu-cHAp and Cu-bHAp

respectively, The first ratio corresponds to calcium deficient hydroxyapatite, the second is very close to the stoichiometric Ca/P ratio of pure hydroxyapatite, 1.67.

According to EDX spectrum of Cu-cHAp sample, there is a major Ti signal relative to Ca and P, implying a thinner or less dense apatite. The second sample shows a dramatically increased Ca and P intensity relative to Ti, confirming the creation of a much thicker apatite layer covering the substrate.

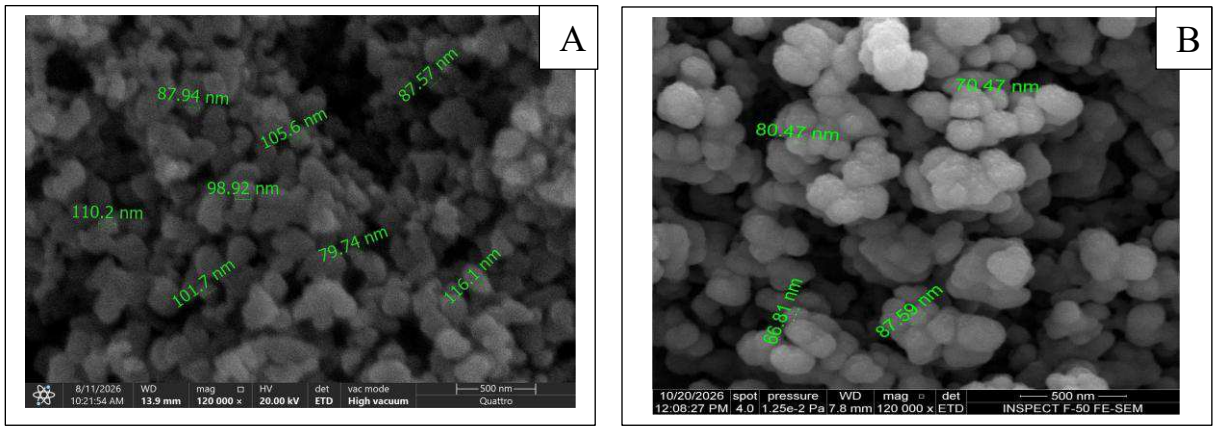
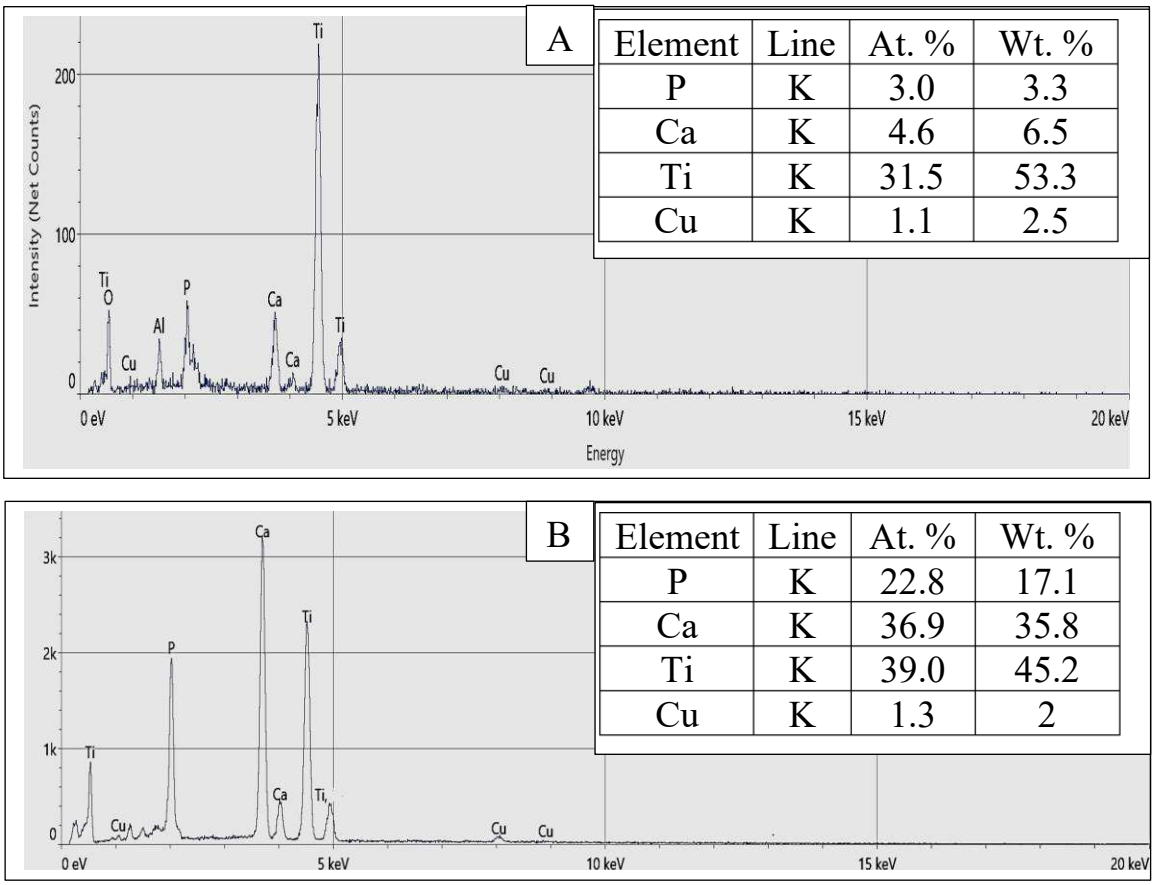


Fig 8. SEM images of A: Cu-cHAp, B: Cu-bHAp after immersing inside SBF



Element	Line	At. %	Wt. %
P	K	3.0	3.3
Ca	K	4.6	6.5
Ti	K	31.5	53.3
Cu	K	1.1	2.5

Element	Line	At. %	Wt. %
P	K	22.8	17.1
Ca	K	36.9	35.8
Ti	K	39.0	45.2
Cu	K	1.3	2

Fig 9. EDX spectrum for A: Cu-cHAp, B: Cu-bHAp

Anticancer Activity

For Cu-cHAp sample, cytotoxicity on MCF7 (Cancer Cells) exhibits a strong, concentration dependent. The killing effect rises progressively, reaching approximately 90% cytotoxicity at the highest concentration of 200µg/mL, see Figure 10(A). Cytotoxicity on HDF (Normal Cells) shows notable and parallel toxicity toward healthy cells as the concentration increases, reaching nearly 45% cytotoxicity at 200µg/mL.

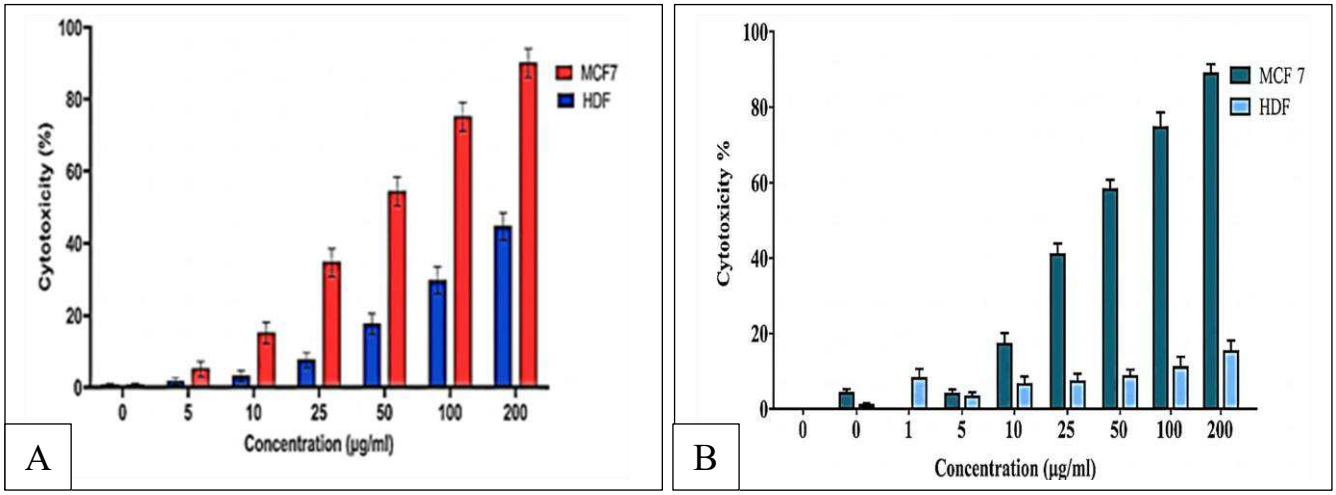


Fig 10. cytotoxicity of A: Cu-nHAp and B: Cu-bHAp on MCF7 and HDF cells across concentrations

On the other hand, cytotoxicity in MCF7 with Cu-bHAp (Figure 10(B)) shows a sharp, potent increase starting at 10µg/mL, reaching a maximum cytotoxic effect of nearly 88–90% at 200µg/mL. Cytotoxicity on HDF remains consistently low across the entire concentration range, remaining below 15% even at 200µg/mL. Cu-bHAp shows high selectivity, effectively destroying cancer cells while preserving the viability of healthy normal cells. Cu-bHAp exhibits a far superior biological profile compared to Cu-nHAp.

Copper ions (Cu^{2+}/Cu+) exhibit dual behavior depending on the cellular environment. In normal cells at lower/moderate doses, they support redox homeostasis (acting as an antioxidant). However, cancer cells naturally exhibit higher baseline oxidative stress and altered metabolic states; the introduction of copper can activate intracellular ROS generation (via Fenton-like reactions) within cancer cells, leading to targeted toxicity [44].

Morphological changes in MCF-7 cells before and after treating with Cu-bHAp are shown in Figure 11.

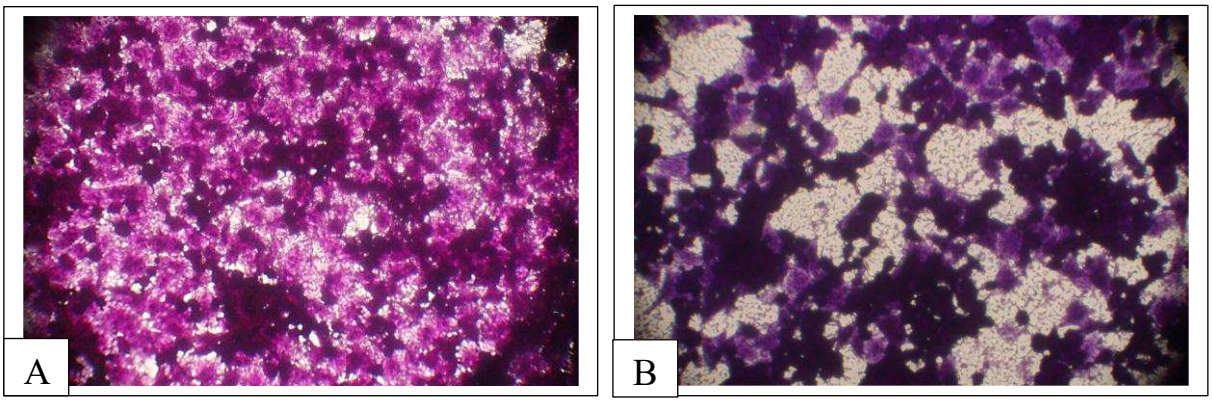


Fig 11. A: Control untreated MCF-7 cells. B: Morphological changes in MCF-7 cells treated with Cu-nHAp.

The picture of control (untreated MCF-7 cells) displays a dense, highly confluent monolayer of intact MCF-7 human breast cancer cells. This morphology shows typical polygonal, epithelial-like shape with sharp, well-defined cell borders. Also, there is homogeneous violet/purple crystal violet staining indicates high metabolic activity, cell viability, and strong adherence to the culture dish surface.

The micrograph of MCF-7 cells after treatment with Cu-nHAp (Figure 11(B)) shows a substantial reduction in total cell population and monolayer integrity, indicating clear cytotoxic effects. There is a loss of normal polygonal structure, shrinking into rounded, condensed remnants. It can observe the formation of large, clear acellular zones ("flatulent spaces") where dead cells detached from the substratum. Also, the morphology illustrates aggregation of fragmented cellular debris and pyknotic nuclear/cytoplasmic remnants.

Inside the acidic tumor microenvironment or lysosomes, copper ions Cu^{2+}/Cu^{+} dissociate from the Cu-bHAp lattice. Cu^{+} reacts with intracellular hydrogen peroxide H_2O_2 through Fenton-like reactions, yielding highly reactive hydroxyl radicals ($^{\bullet}OH$): $Cu^{+} + H_2O_2 \rightarrow Cu^{2+} + {}^{\bullet}OH + OH^{-}$. Excessive ROS triggers lipid peroxidation, mitochondrial membrane breakdown, and DNA damage, causing programmed cell death (apoptosis/cuproptosis) [26].

Conclusions

1- Incorporating Cu^{2+} into hydroxyapatite preserves the fundamental crystal framework, but high-temperature calcination triggers partial decomposition into tricalcium phosphate (TCP). This biphasic transformation is far more pronounced in catfish-derived Cu-bHAp due to lattice destabilization caused by native biogenic co-dopants Mg^{2+}, Na^{+}, CO_3^{2-}.

2- Synthetic Cu-cHAp functions as a potent antioxidant and broad-spectrum antimicrobial agent because its unconstrained lattice allows rapid copper ion diffusion and surface redox cycling Cu^{2+}/Cu^{+}. Conversely, the complex biogenic matrix and secondary TCP sub-phase in Cu-bHAp structurally encapsulate the copper species, hindering active ion release into surrounding media.

3- Fishbone-derived Cu-bHAp exhibits superior bioactivity and faster apatite layer nucleation upon immersion in SBF compared to Cu-cHAp. This is driven by its higher proportion of labile TCP, which lowers the thermodynamic energy barrier for local calcium and phosphate ion release.

4- Bio-extracted Cu-bHAp achieves exceptional biological selectivity, destroying MCF-7 breast cancer cells via acid-triggered Fenton-like ROS generation. Unlike synthetic Cu-cHAp , which exhibits significant off-target cytotoxicity against normal fibroblasts, Cu-bHAp restricted release kinetics protect healthy tissues while eliminating malignant cells.

ACKNOWLEDGEMENTS

The authors acknowledge Mustansiriyah university for the support.

Statements and Declarations

The authors have no competing interests to declare that are relevant to the content of this article.

funding

No funding was received to assist with the preparation of this manuscript.

Financial interests

The authors declare they have no financial interests.

Ethics declaration: not applicable.

References

1. Shi P, Liu M, Fan F, Yu C, Lu W, Du M (2018) Characterization of natural hydroxyapatite originated from fish bone and its biocompatibility with osteoblasts. Mater Sci Eng C 90:706-712. https://doi.org/10.1016/j.msec.2018.04.096

2. Bazin T, Magnaudeix A, Mayet R, Carles P, Julien I, Demourgues A, Gaudon M, Champion E (2021) Sintering and biocompatibility of copper-doped hydroxyapatite bioceramics. Ceram Int 47:13644-13654. https://doi.org/10.1016/j.ceramint.2021.01.225

3. Anand A, Kaňková H, Hájovská Z, Galusek D, Boccaccini AR, Galusková D (2024) Bioresponse of copper-magnesium co-substituted mesoporous bioactive glass for bone tissue regeneration. J Mater Chem B 12:1875-1891. https://doi.org/10.1039/D3TB02102A

4. Ghosh R, Swart O, Westgate S, Miller BL, Yates MZ (2019) Antibacterial copper–hydroxyapatite composite coatings via electrochemical synthesis. Langmuir 35:5957-5966. https://doi.org/10.1021/acs.langmuir.9b00919

5. Unabia RB, Candidato RT Jr, Pawłowski L, Salvatori R, Bellucci D, Cannillo V (2020) In vitro studies of solution precursor plasma-sprayed copper-doped hydroxyapatite coatings with increasing copper content. J Biomed Mater Res Part B Appl Biomater 108:2579-2589. https://doi.org/10.1002/jbm.b.34589

6. Kubiak K, Klimczak A, Dziki L, Modranka R, Malinowska K (2010) Influence of copper (II) complex on the activity of selected oxidative enzymes. Pol Merkur Lekarski 28:22-25

7. Li B, Yu S (2007) In vitro study of the effects of copper ion on osteoclastic resorption in various dental mineralized tissues. Chin J Stomatol 42:110-113

8. Ciosek Ż, Kot K, Rotter I (2023) Iron, zinc, copper, cadmium, mercury, and bone tissue. Int J Environ Res Public Health 20:2197. https://doi.org/10.3390/ijerph20032197

9. Ressler A, Žužević A, Ivanišević I, Kamboj N, Ivanković H (2021) Ionic substituted hydroxyapatite for bone regeneration applications: A review. Open Ceram 6:100122. https://doi.org/10.1016/j.oceram.2021.100122

10. Ciobanu CS, Predoi D, Iconaru SL, Predoi MV, Ghegoiu L, Buton N, Motelica-Heino M (2024) Copper doped hydroxyapatite nanocomposite thin films: synthesis, physico–chemical and biological evaluation. Biometals 37:1487-1500. https://doi.org/10.1007/s10534-024-00609-3

11. Wu C, Zhou Y, Xu M, Han P, Chen L, Chang J, Xiao Y (2013) Copper containing mesoporous bioactive glass scaffolds with multifunctional properties of angiogenesis capacity, osteostimulation and antibacterial activity. Biomaterials 34:422-433. https://doi.org/10.1016/j.biomaterials.2012.09.066

12. Frangoulis M, Georgiou P, Chrisostomidis C, Perea D, Dontas I, Kavantzas N, Kostakis A, Papadopoulos O (2007) Rat epigastric flap survival and VEGF expression after local copper application. Plast Reconstr Surg 119:837-843. https://doi.org/10.1097/01.prs.0000252000.59231.5e

13. Boutinguiza M, Comesaña R, Lusquiños F, Riveiro A, Pou J (2011) Production of nanoparticles from natural hydroxylapatite by laser ablation. Nanoscale Res Lett 6:255. https://doi.org/10.1186/1556-276X-6-255

14. Huang YC, Hsiao PC, Chai HJ (2011) Hydroxyapatite extracted from fish scale: effects on MG63 osteoblast-like cells. Ceram Int 37:1825-1831. https://doi.org/10.1016/j.ceramint.2011.01.037

15. Sunil BR, Jagannatham M (2016) Producing hydroxyapatite from fish bones by heat treatment. Mater Lett 185:411-414. https://doi.org/10.1016/j.matlet.2016.09.039

16. Mondal S, Mahata S, Kundu S, Mondal B (2010) Processing of natural resourced hydroxyapatite ceramics from fish scale. Adv Appl Ceram 109:234-239. https://doi.org/10.1179/174367509X12500913619934

17. Boutinguiza M, Pou J, Comesaña R, Lusquiños F, de Carlos A, León B (2012) Biological hydroxyapatite obtained from fish bones. Mater Sci Eng C 32:478-486. https://doi.org/10.1016/j.msec.2011.11.021

18. Anand A, Kaňková H, Hájovská Z, Galusek D, Boccaccini AR, Galusková D (2024) Bioresponse of copper-magnesium co-substituted mesoporous bioactive glass for bone tissue regeneration. J Mater Chem B 12:1875-1891. https://doi.org/10.1039/D3TB02102A

19. Weiss KM, Kucko SK, Mokhtari S, Keenan TJ, Wren AW (2023) Investigating the structure, solubility, and antibacterial properties of silver- and copper-doped hydroxyapatite. J Biomed Mater Res B Appl Biomater 111:295-313. https://doi.org/10.1002/jbm.b.35151

20. Claudel M, Schwarte JV, Fromm KM (2020) New antimicrobial strategies based on metal complexes. Chemistry 2:849-899. https://doi.org/10.3390/chemistry2040055

21. Shen Q, Qi Y, Kong Y, Bao H, Wang Y, Dong A, Wu H, Xu Y (2022) Advances in copper-based biomaterials with antibacterial and osteogenic properties for bone tissue engineering. Front Bioeng Biotechnol 10:795425. https://doi.org/10.3389/fbioe.2022.795425

22. Slavin YN, Asnis J, Häfeli UO, Bach H (2017) Metal nanoparticles: Understanding the mechanisms behind antibacterial activity. J Nanobiotechnol 15:65. https://doi.org/10.1186/s12951-017-0308-z

23. Crisan MC, Teodora M, Lucian M (2022) Copper nanoparticles: Synthesis and characterization, physiology, toxicity and antimicrobial applications. Appl Sci 12:141. https://doi.org/10.3390/app12010141

24. Fan X, Yahia LH, Sacher E (2021) Antimicrobial properties of the Ag, Cu nanoparticle system. Biology 10:137. https://doi.org/10.3390/biology10020137

25. Bădilă AE, Rădulescu DM, Ilie A, Niculescu AG, Grumezescu AM, Rădulescu AR (2022) Bone regeneration and oxidative stress: An updated overview. Antioxidants 11:318. https://doi.org/10.3390/antiox11020318

26. Benali Y, et al (2024) Physico-chemical properties of copper-doped hydroxyapatite coatings obtained by vacuum deposition technique. Materials 17:3681. https://doi.org/10.3390/ma17153681

27. Kumar R, Topno U, Shikha D, Anand S, Sinha SK, Mohanty PK, Mhaske S (2025) High antioxidant activity, enhanced cytocompatibility, improved apatite formation, and moderate thrombogenicity of copper-doped hydroxyapatite attributed to structural changes analysed using EDX, FTIR, XRD, and FESEM. BioNanoScience 15:323. https://doi.org/10.1007/s12668-024-01350-4

28. Saghiri MA, Asatourian A, Orangi J, Sorenson CM, Sheibani N (2015) Functional role of inorganic trace elements in angiogenesis-Part II: Cr, Si, Zn, Cu, and S. Crit Rev Oncol Hematol 96:143-155. https://doi.org/10.1016/j.critrevonc.2015.05.011

29. Venkatesan J, Bhatnagar I, Manivasagan P, Kang KH, Kim SK (2015) Alginate composites for bone tissue engineering: a review. Int J Biol Macromol 72:269-281. https://doi.org/10.1016/j.ijbiomac.2014.07.008

30. Noori A, Hoseinpour M, Kolivand S, Lotfibakhshaiesh N, Ebrahimi-Barough S, Ai J, Azami M (2024) Exploring the various effects of Cu doping in hydroxyapatite nanoparticle. Sci Rep 14:3421. https://doi.org/10.1038/s41598-024-53704-x

31. Abbas MK, Hashim MS (2023) Investigation of biomimetic hydroxyapatite formation on titania nanoparticles and lobed nanotubes. Kuwait J Sci 50:1-9

32. Hashim MS, Al Marjani MF, Hussein TS, Kh RS, Kh ZA, J AS (2019) Jordan J Biol Sci 12:415-419

33. Naser DM, Lafta SH, Hashim MS (2023) Effect of hydrothermal reaction time on structure, magnetic, and biological properties of iron sulfide nanoparticles. ChemistrySelect 8:e202301568. https://doi.org/10.1002/slct.202301568

34. Eremina NV, Bulina NV, Mikhailenko MA, Vinokurova OB, Prosanov IY, Chaikina MV (2023) Cu-substituted hydroxyapatite powder: Mechanochemical synthesis using different copper sources and thermal stability. Powders 2:678-696. https://doi.org/10.3390/powders2040042

35. Gopi D, Indira J, Kavitha L (2012) A comparative study on the direct and pulsed current electrodeposition of hydroxyapatite coatings on surgical grade stainless steel. Surf Coat Technol 206:2859-2869. https://doi.org/10.1016/j.surfcoat.2011.12.016

36. Fiume E, Magnaterra G, Rahdar A, Verné E, Baino F (2021) Hydroxyapatite for biomedical applications: A short overview. Ceramics 4:542-563. https://doi.org/10.3390/ceramics4040039

37. Predoi D, Iconaru SL, Ciobanu SC, Rokosz K, Raaen S, Țălu Ș (2026) Structural, surface, and biological evaluation of copper-doped hydroxyapatite coatings synthesized via an adapted sol-gel method. Mater Sci Eng B 329:119473. https://doi.org/10.1016/j.mseb.2024.119473

38. Anand S, Sinha SK (2024) Mechanical, structural, corrosion, and dielectric properties of hydroxyapatite doped with varying concentrations of Cu to be used as orthopedic implants. J Mater Eng Perform 33:14368-14380. https://doi.org/10.1007/s11665-023-08970-7

39. Kubiak-Mihkelsoo Z, Kostrzębska A, Błaszczyszyn A, Pitułaj A, Dominiak M, Gedrange T, Nawrot-Hadzik I, Matys J, Hadzik J (2025) Ionic doping of hydroxyapatite for bone regeneration: Advances in structure and properties over two decades—A narrative review. Appl Sci 15:1108. https://doi.org/10.3390/app15031108

40. Kim TN, Feng QL, Kim JO, Wu J, Wang H, Chen GC, Cui FZ (1998) Antimicrobial effects of metal ions (Ag+, Cu2+, Zn2+) in hydroxyapatite. J Mater Sci Mater Med 9:129-134. https://doi.org/10.1023/a:1008811501734

41. Vincent M, Duval RE, Hartemann P, Engels-Deutsch M (2018) Contact killing and antimicrobial properties of copper. J Appl Microbiol 124:1032-1046. https://doi.org/10.1111/jam.13681

42. Noori A, Hoseinpour M, Kolivand S, Lotfibakhshaiesh N, Ebrahimi-Barough S, Ai J, Azami M (2024) Exploring the various effects of Cu doping in hydroxyapatite nanoparticle. Sci Rep 14:3421. https://doi.org/10.1038/s41598-024-53704-x

43. Granito RN, Renno ACM, Yamamura H, de Almeida MC, Ruiz PLM, Ribeiro DA (2018) Hydroxyapatite from fish for bone tissue engineering: A promising approach. Int J Mol Cell Med 7:80-90

44. Vo TTT, Peng TY, Nguyen TH, Bui TNH, Wang CS, Lee WJ, Chen YL, Wu YC, Lee IT (2024) The crosstalk between copper-induced oxidative stress and cuproptosis: a novel potential anticancer paradigm. Cell Commun Signal 22:353. https://doi.org/10.1186/s12964-024-01730-x